

Characterization of Al₂O₃-Supported Manganese Oxides by Electron Spin Resonance and Diffuse Reflectance Spectroscopy

W. Sjoerd Kijlstra, Eduard K. Poels, and Alfred Bliek*

Department of Chemical Engineering, University of Amsterdam, Nieuwe Achtergracht 166,
1018 WV Amsterdam, The Netherlands

Bert M. Weckhuysen and Robert A. Schoonheydt

Center for Surface Chemistry and Catalysis, KU Leuven, Kardinaal Mercierlaan 92, 3001 Heverlee, Belgium

Received: August 2, 1996; In Final Form: October 23, 1996[⊗]

Alumina-supported manganese oxides, used as catalysts for the selective catalytic reduction of NO, were characterized by combined electron spin resonance and diffuse reflectance spectroscopies. Upon impregnation of the acetate precursor solution, the [Mn(H₂O)₆]²⁺ complex interacts strongly with surface hydroxyls of the γ -Al₂O₃. Evidence was obtained that this anchoring reaction proceeds at a Mn/OH = 1/2 ratio up to 4.5 wt % Mn loading, leading to a highly dispersed oxidic manganese layer. At higher loadings, the precursor complex is deposited on the surface concurrently. Upon drying at 383 K, part of the manganese is oxidized to higher oxidation states (Mn³⁺ and Mn⁴⁺), while a further increase in (average) oxidation state takes place upon calcination at 573 K. After calcination, the manganese species are present as a mixture of Mn²⁺, Mn³⁺, and Mn⁴⁺. At low loadings (<1 wt %), approximately equal amounts of these three oxidation states are present, whereas Mn³⁺ becomes the predominant species at higher loadings. ESR reveals that at low loadings, almost all the manganese is present as isolated species, while at 4.5 wt % Mn loading, still more than 70% of the manganese is isolated. The decrease of the fraction of isolated manganese species at higher loadings is accompanied by a decreased selectivity toward N₂ production in the selective catalytic reduction of NO. The fraction Mn²⁺ is present in an axially distorted octahedral coordination.

1. Introduction

Pure or supported manganese oxides have been used as catalysts for a variety of chemical reactions such as oxidation reactions,^{1–3} the catalytic combustion of methane⁴ and VOC,⁵ nitrous oxide decomposition,⁶ and ozone decomposition.⁵ Besides, alumina-supported manganese oxides perform very well as catalysts for the selective catalytic reduction (SCR) of NO with NH₃.^{7–9}

Compared to its catalytic applications, much less attention has been paid to the characterization of supported manganese oxides. Alumina-supported catalysts were studied by X-ray diffraction (XRD),^{1,4,6,10,11} temperature-programmed reduction (TPR),^{4,7,11} X-ray photoelectron spectroscopy (XPS),^{10,11} low-energy ion scattering (LEIS),¹⁰ infrared spectroscopy (IR),¹² magnetic susceptibility,¹³ and electron spin resonance (ESR).^{14,15} Recently, the characterization of alumina-supported manganese oxides, prepared from the acetate precursor, by XRD, TPR, IR, Raman spectroscopy, and XPS, was discussed by Kapteijn *et al.*¹⁶ They concluded that the synthesis route *via* the acetate precursor yields a highly dispersed manganese oxide phase having a strong interaction with the support, as reflected by the absence of X-ray diffraction lines (up to 8.4 wt % Mn), the shift to higher temperature of the reduction peaks in TPR, and the shift to higher binding energy with respect to the pure oxides, as observed in XPS. In addition, it was shown using TPR that the average oxidation state is approximately 3+ for these catalysts.

However, some questions about the nature of the catalytically active manganese site remain unresolved. Firstly, it is not clear

whether the manganese oxide is present in the form of one oxidation state or in the form of a mixture of oxidic phases. Secondly, the coordination of the manganese has not been elucidated so far. Thirdly, it is not clear whether the Mn atoms are present as isolated species or as two dimensional clusters. As was observed previously,¹⁶ the manganese oxide phase is deposited on the surface as a dispersed phase without microcrystallites. In this study, it will be shown that the catalytic properties with respect to the selectivity of the SCR reaction change considerably between 2 and 4.5 wt % Mn loading. An explanation, assuming the presence of isolated species and two-dimensional clusters, will be discussed.

As the abovementioned questions are important for the elucidation of the catalytically active cycle, an extended characterization study was performed using diffuse reflectance spectroscopy (DRS) and ESR. ESR is able to detect paramagnetically isolated species and gives information about the coordination of isolated sites; consequently, it is very useful to study low-loaded catalysts. ESR is able to detect Mn²⁺ and Mn⁴⁺, whereas Mn³⁺ is usually not detected.¹⁷ In the UV–vis region of the DRS spectra, the d–d transitions of Mn³⁺ and Mn⁴⁺ can be seen,^{18,19} whereas the transitions of Mn²⁺ are all spin forbidden and by consequence very weak. Moreover, the near-infrared region of the DRS spectra can be used to obtain evidence for the anchoring of Mn ions to surface hydroxyls of the Al₂O₃ support, as previously proposed on the basis of IR studies,¹⁶ in a more quantitative way.

Therefore, combined ESR–DRS spectroscopies seem to be suited to address the abovementioned questions.

2. Experimental Section

2.1. Materials. The catalysts were prepared by incipient wetness impregnation of a Ketjen CK300 γ -Al₂O₃ support (*S*_{BET}

* To whom correspondence should be addressed. Fax: +31 20 5255604.
E-mail: bliek@chemeng.chem.uva.nl.

[⊗] Abstract published in *Advance ACS Abstracts*, December 15, 1996.

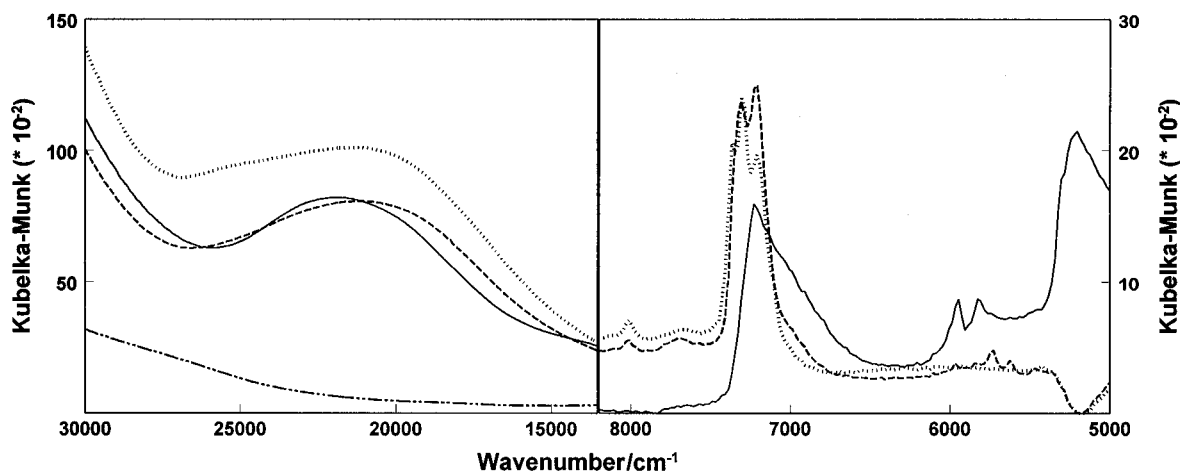


Figure 1. DRS spectra of 0.5 wt % Mn/Al₂O₃ after (a) drying at 383 K (—), (b) calcination in O₂ at 573 K (---), and (c) calcination at 773 K (···). DRS spectrum of γ -Al₂O₃ (d) after calcination at 773 K (- · - ·).

= 200 m² g⁻¹, pore volume 0.5 cm³ g⁻¹, and particle size 150–250 μ m) with an aqueous solution of (CH₃COO)₂Mn·4H₂O. Subsequently, the catalysts were dried in stagnant air overnight at 383 K, followed by calcination in O₂ at 573 K for 1 h and at 773 K for 3 h. Due to the limited solubility of the precursor, the impregnation was performed in several steps with drying in-between (except for the 0.5 wt % catalyst). In this way, samples were prepared ranging from 0.5 to 8 wt % Mn loading. For several dried samples, the calcination procedure was evaluated by spectroscopy.

The gases used were all supplied by Air Liquide. During the experiments, the samples were fixed in a quartz flow cell containing an optical Suprasil window for DRS and a capillary side arm for ESR. After all treatments, the cell was disconnected from the flow system and sealed, and subsequently, spectra were taken.

2.2. Characterization Techniques. UV-vis spectra of the aqueous solution of the precursor Mn(CH₃COO)₂·4H₂O were recorded on a Perkin-Elmer Lambda 12 spectrophotometer in the 200–900-nm range. The spectra exactly match the published spectra of the [Mn(H₂O)₆]²⁺ complex.²⁰

DRS spectra were recorded on a Varian Cary 5 UV-vis-near-IR spectrophotometer at room temperature in the range 200–2500 nm. A Halon white reflectance standard was subtracted as background. From all absorption spectra, the Kubelka-Munk function was automatically calculated. Further spectral processing was performed using the software package GRAMS/386 (Galaxy Industrial Corp.).

ESR spectra were recorded on a Bruker ESP 300E instrument, mainly in the X band at a microwave power of 200 μ W with a double-rectangular TE₁₀₄ mode cavity, connected to liquid nitrogen or helium cooling equipment. Besides, a few spectra were recorded in the Q band and K band. The software allows double integration of the spectra and therefore the calculation of spin densities, using (CH₃COO)₂Mn·4H₂O/KCl mixtures, with spin densities ranging from 10¹⁹ to 10²¹ spins g⁻¹, as reference materials. Typically, the samples were measured at 140–150 K, but some were measured down to 20 K. Before recording the spectra, the samples were flushed with He to remove weakly adsorbed oxygen. Spectral simulations were performed with the software package QPOW.²¹

2.3. Catalytic Tests. The selectivity toward N₂ production for the selective catalytic reduction of NO with NH₃ of 1–8 wt % Mn/Al₂O₃ samples was determined at 523 K, using a standard flue gas mixture. The experimental details of the equipment and procedure were described previously.^{7,8}

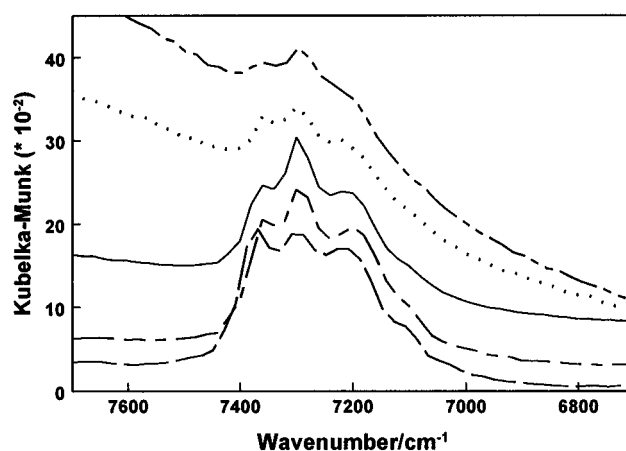


Figure 2. DRS spectra of γ -Al₂O₃-supported manganese oxides after calcination in O₂ at 773 K; γ -Al₂O₃ (- · - ·), 0.5 wt % Mn (- - -), 2 wt % Mn (—), 4.5 wt % Mn (···), and 7 wt % Mn (- · - ·).

3. Results

3.1. Diffuse Reflectance Spectroscopy. Dried and Cal-

culated Samples. As an example, the spectra of the 0.5 wt % Mn/Al₂O₃ catalyst as a function of calcination temperature are shown in Figure 1. A spectrum of the calcined Al₂O₃ support is presented as well. The freshly dried sample exhibits a Mn band at 21 700–22 000 cm⁻¹, partly covered by strong but unresolved charge-transfer bands at 35 000–40 000 cm⁻¹ (not shown).¹⁸ In the near-infrared region, overtones of the acetate precursor (2 ν of the C–H vibration) are observed at 5820 and 5940 cm⁻¹.²² Moreover, the first overtone (2 ν) of molecularly adsorbed water (6800 cm⁻¹) can be seen, accompanied by a combination band ($\nu + \delta$) at 5200 cm⁻¹.²³

Upon calcination at 373 K, the band of molecularly adsorbed water disappears. The acetate decomposes between 473 and 573 K (Figure 1b). At 573 K, the Mn band has shifted toward 21 000 cm⁻¹. Moreover, the first overtones of surface hydroxyls of the Al₂O₃ support are resolved in the region 7100–7360 cm⁻¹.²²

Upon calcination at 773 K (Figure 1c), the intensity of the Mn band has increased considerably and is centered at 21 200 cm⁻¹, with a weak shoulder around 25 000 cm⁻¹. The surface hydroxyls are well pronounced in the spectrum at 7210, 7290, and 7360 cm⁻¹, assigned to the overtones of acidic, neutral, and basic hydroxyls, respectively.²⁴

The spectra of higher loaded (2–7 wt %) samples show comparable changes during calcination. The Mn band, observed

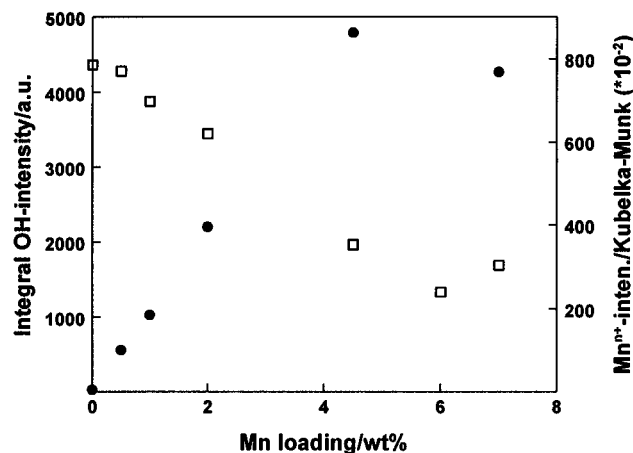


Figure 3. Integrated intensities of DRS bands in the OH region (\square) and line heights of the DRS band Mn^{2+} region (\bullet) after calcination at 773 K in O_2 as a function of Mn loading.

in the range 20 900–22 000 cm^{-1} , is reflected at these loadings in the form of a shoulder of the band at 40 000 cm^{-1} . Usually the rise in intensity, as observed between 573 and 773 K for the 0.5 wt % loaded sample, proceeds at approximately 573 K for the higher loaded samples. The main difference between the spectra of higher loaded samples and the 0.5 wt % loaded sample is found in the intensity of the Mn band and the bands of the surface hydroxyls (Figure 3). For a low concentration of absorbing centers, the Kubelka–Munk law predicts a linear correlation between $F(R_\infty)$ and this concentration. Hence, a quantitative evaluation of the spectra is possible. Figure 3 shows the intensities of the Mn band and of the surface hydroxyls as a function of Mn loading. Up to 4.5 wt % loading, the intensity of the Mn band increases linearly with loading; it should be mentioned that at higher loadings, the Kubelka–Munk law is no longer valid. The bands (from 6900 to 7600 cm^{-1}) of the overtones of the surface hydroxyls were integrated after subtraction of a linear background. For the highest loadings, this method is less accurate (see Figure 2). Clearly, the integrated intensity of the hydroxyls decreases linearly with loading up to 4.5 wt % Mn; beyond this loading, the intensity remains constant. Thus, the increase of the Mn absorption band is accompanied by a decrease of the OH peaks in the near-infrared region.

Reduced Samples. During reduction, the color of the sample progressively changes from pale pink to brown (depending on Mn loading) before reduction to white after reduction at 930 K. The spectral range of the Mn band of 2 wt % $\text{Mn}/\text{Al}_2\text{O}_3$ during reduction by H_2 is shown in Figure 4. Before reduction, the sample was dehydrated in O_2 at 573 K: the spectrum shows a band in the range 21 500–22 800 cm^{-1} (band 1). Moreover, a very weak feature is observed around 25 000 cm^{-1} . Upon reduction at 473 K, the maximum of band 1 is at 21 900 cm^{-1} . The weak band already found after dehydration becomes a band with a maximum at 25 600 cm^{-1} (band 2). The intensity of the entire spectrum is reduced in this range. Upon reduction at 573 K, the entire spectrum is considerably less intense. The maximum of band 2 is slightly more pronounced. The maximum of band 1 is shifted slightly upwards. After reduction at 673 K, the intensity of the entire spectrum is significantly reduced. Both bands can still be observed, at a slightly higher wavenumber. At 930 K, only one very weak but sharp band with a maximum at 23 700 cm^{-1} is observed, shown more clearly in the insert of Figure 4.

3.2. Electron Spin Resonance. Dried and Calcined Samples. As an example, ESR spectra of 0.5 wt % $\text{Mn}/\text{Al}_2\text{O}_3$ at different stages of calcination are shown in Figure 5. The

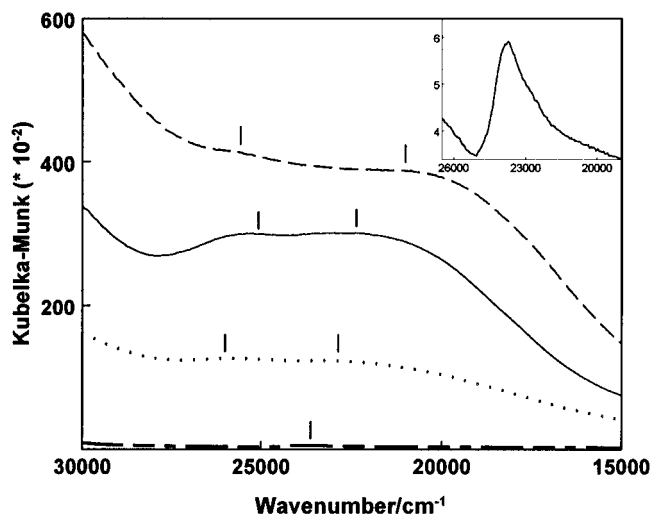


Figure 4. DRS spectra of 2 wt % $\text{Mn}/\text{Al}_2\text{O}_3$ after calcination at 773 K (---), reduction by H_2 at 573 K (—), 673 K (···), and 930 K (— · —). In the insert: details of the spectrum after reduction at 930 K.

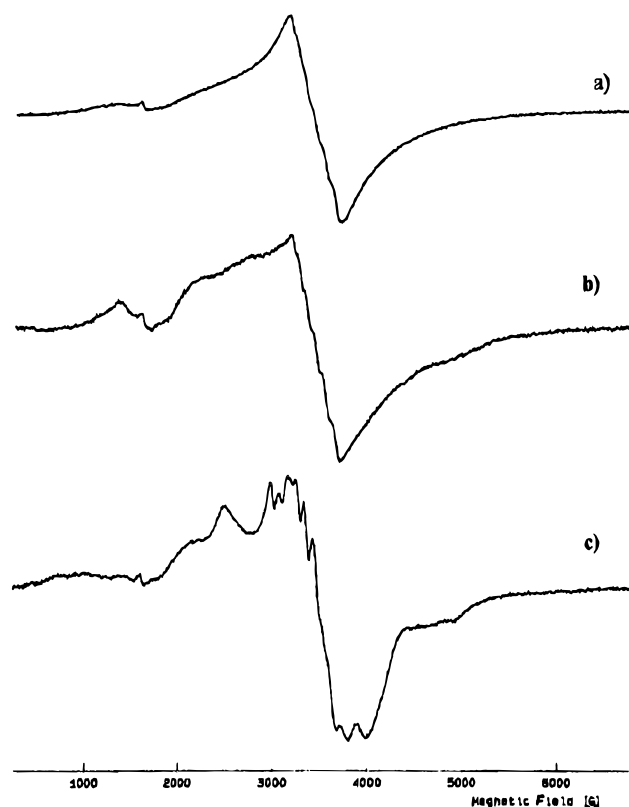


Figure 5. ESR spectra (X band) of 0.5 wt % $\text{Mn}/\text{Al}_2\text{O}_3$ after (a) drying at 383 K, (b) calcination in O_2 at 573 K, and (c) 773 K.

dried sample shows a broad signal with $g = 2.0119$ exhibiting “wings” on both sides, and a poorly resolved six-line hyperfine structure with splitting constant $A = 78.1(\pm 3.9) \times 10^{-4} \text{ cm}^{-1}$. The latter signal appears to be isotropic, suggesting an octahedral/tetrahedral symmetry of the paramagnetic Mn ion. A small Fe^{3+} impurity is visible at $g = 4.3$. Upon calcination at 573 K, the values of g and A slightly change (2.0189 and $78.1(\pm 3.9) \times 10^{-4} \text{ cm}^{-1}$, respectively). Fine structure lines are found at higher and lower field, indicating a change to axial symmetry. After calcination at 773 K, both the hyperfine and the fine structure become better resolved. The spectrum is characterized by a g value of 2.0012 and a hyperfine splitting constant A of $82.3(\pm 4.1) \times 10^{-4} \text{ cm}^{-1}$. A rough estimate of the zero-field splitting parameter D , extracted from the distance between the central sextet and the outer sextets,²⁵ yields a value of

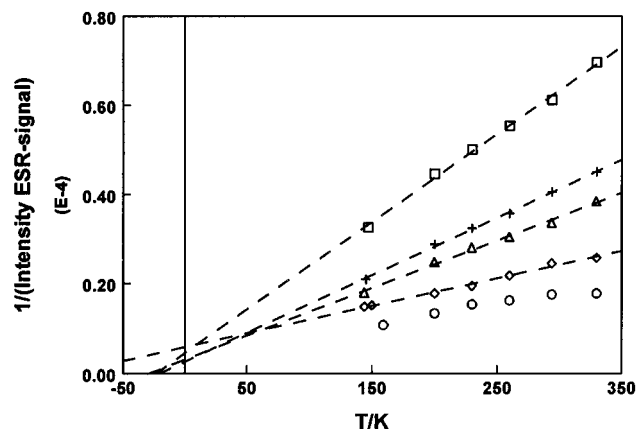


Figure 6. Curie–Weiss plots ($1/\text{intensity ESR signal}$ vs temperature) of calcined $\gamma\text{-Al}_2\text{O}_3$ -supported manganese oxides: 0.5 wt % Mn (\square), 2 wt % Mn ($+$), 4.5 wt % Mn (\triangle), 6 wt % Mn (\diamond), and 7 wt % Mn (\circ).

$550(\pm 27.5) \times 10^{-4} \text{ cm}^{-1}$. This signal is superimposed on a broad isotropic signal (wings), already present in the spectra of the dried sample. Computer simulations indicate that the spectrum cannot be constructed by assuming only one paramagnetic species.

At higher loadings, both the hyperfine structure and the fine structure are much less resolved, with values of g and A not being significantly different from those determined at 0.5 wt % loading. The broad, isotropic signal, superimposed by the central sextet, also remains unchanged at higher loadings. Some additional spectra of a 2 wt % Mn/ Al_2O_3 sample were recorded in the Q band and K band. From these spectra, it was possible to determine A more exactly, but they yielded no new fine structure. These spectra were also recorded down to liquid He temperature; however, no qualitative changes with temperature were observed.

The total intensity of the ESR signal provides more quantitative information. Isolated paramagnetic species follow the Curie–Weiss law, giving a linear relation between the intensity of the signal and the reciprocal temperature:

$$\chi_{\text{Mn}^{n+}} = \frac{C}{T - \theta} \propto I_{\text{Mn}^{n+}} \quad (1)$$

in which χ = magnetic (molar) susceptibility, C = Curie constant, and θ = Weiss constant.

Hence, recording spectra at different temperatures provides evidence as to the presence of isolated paramagnetic species.

The intensities of the ESR signals of 0.5–7 wt % Mn/ Al_2O_3 , measured between 140 and 330 K, were double integrated over the total magnetic field range. The values obtained by integration have uncertainty limits of $\pm 5\%$. The reciprocal intensity was plotted against temperature (Figure 6). Clearly, straight lines can be fitted up to 4.5 wt % Mn loading. Assuming that these straight lines may be extrapolated to lower temperatures (spectra in the Q band and K band at 20 K do not show different features), this means that at least part of the manganese is present as isolated paramagnetic species. By extrapolation, the values of θ can be obtained, reflecting the deviation from ideal magnetic behavior. If species are perfectly isolated, θ is close to 0. The obtained values are comparable for the 0.5–4.5 wt % loaded samples and deviate less than 25 K from 0. In contrast, at 6 wt % loading, a straight line can be fitted, but the value of θ is far from 0, indicating that the manganese species show no Curie–Weiss behavior. At the highest loading, all manganese species are magnetically influenced by each other and no linear dependency is observed.

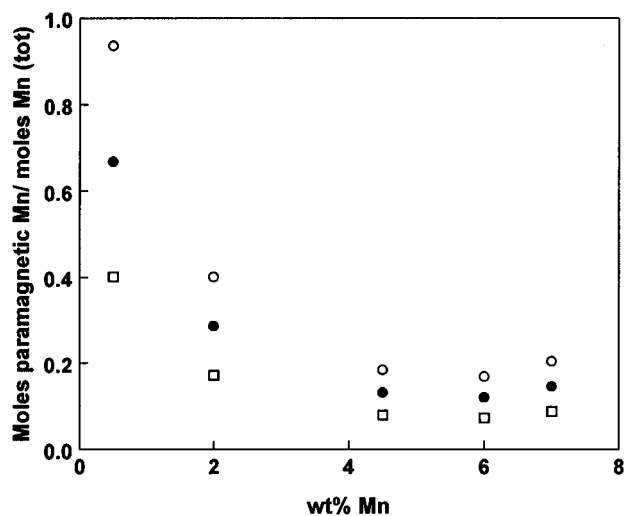


Figure 7. Molar fraction paramagnetic Mn of calcined $\gamma\text{-Al}_2\text{O}_3$ -supported manganese oxides as a function of Mn loading if all the ESR signal is due to Mn^{2+} (\square), Mn^{4+} (\circ), and a 1:1 mixture of Mn^{2+} and Mn^{4+} (\bullet).

The amount of spins per mole of manganese at different Mn loadings was determined, according to eq 2, using calibration mixtures of manganese acetate, diluted by KCl. Mn ions can be observed by ESR as Mn^{2+} ($S = 3/2$) and Mn^{4+} ($S = 5/2$). The spin quantum number S determines the intensity of the signal of 1 mole of paramagnetic atoms; by consequence, the ESR signal of 1 mol of Mn^{4+} is $7/3$ times the ESR signal of 1 mol of Mn^{2+} ;

$$N_{\text{Mn}^{n+}} = N_{\text{ref}} \frac{A_{\text{Mn}^{n+}}}{A_{\text{ref}}} \frac{g_{\text{ref}}}{g_{\text{Mn}^{n+}}} \frac{S_{\text{ref}}(S_{\text{ref}} + 1)}{S_{\text{Mn}^{n+}}(S_{\text{Mn}^{n+}} + 1)} \quad (2)$$

in which $N_{\text{Mn}^{n+}}$ and N_{ref} = amount of spins of Mn^{n+} and the reference sample, respectively, $A_{\text{Mn}^{n+}}$ and A_{ref} = integrated intensity of the ESR signal of Mn^{n+} and the reference sample, respectively, $g_{\text{Mn}^{n+}}$ and $g_{\text{ref}} = g$ value of Mn^{n+} and the reference sample, respectively, $S_{\text{Mn}^{n+}}$ and S_{ref} = spin quantum number of Mn^{n+} and the reference sample, respectively. Figure 7 shows the molar fraction of paramagnetic Mn species vs the Mn loading for three cases: two extreme cases in which all paramagnetic species are supposed to be Mn^{2+} or Mn^{4+} , respectively, and one intermediate case in which a ratio of $\text{Mn}^{2+}/\text{Mn}^{4+} = 1$ is assumed. As a Mn^{3+} average oxidation state was estimated from TPR,¹⁶ a molar ratio $\text{Mn}^{2+}/\text{Mn}^{4+} = 1$ would represent the fraction of paramagnetic manganese species most reasonably. At 0.5 wt % Mn, about two-thirds of the manganese present is accessible by ESR. Clearly, the signal per mole of manganese decreases sharply from 0.5 to 4.5 wt % loading and remains constant at higher loadings.

Reduced Samples. ESR spectra of the 0.5–4.5 wt % Mn/ Al_2O_3 samples were recorded after reduction at increasing temperatures. The hyperfine structure and fine structure in the spectra of dehydrated samples become less resolved during the reductive treatment, whereas no new absorption lines are observed. After reduction at 930 K, the spectra consist of one isotropic signal. As an example, the spectrum of 2 wt % Mn/ Al_2O_3 is shown in Figure 8. The intensity of the signal strongly increases with reduction temperature. As the amount of Mn^{2+} increases upon reduction, these higher ESR signals are in agreement with eq 2. Besides, the increased amount of Mn^{2+} will result in relatively less diluted Mn^{2+} species, explaining the disappearance of the fine structure and hyperfine structure. As the spectra of the reduced samples have the same structure

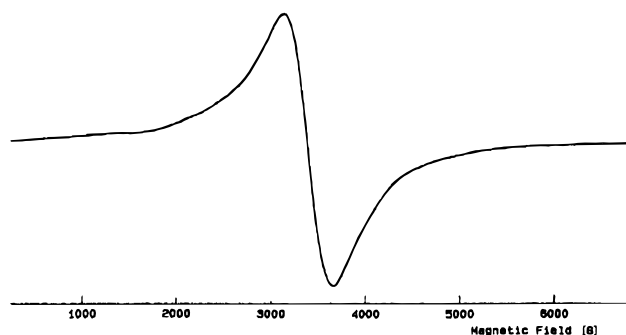


Figure 8. ESR spectrum (X band) of 2 wt % Mn/Al₂O₃ after reduction in H₂ at 930 K.

TABLE 1: Detected Paramagnetic Manganese Species before and after Reduction at 930 K

loading/wt %	fraction of paramagnetic Mn	
	before reduction ^a	after reduction
0.5	0.67	0.97
2	0.29	0.82
4.5	0.13	>0.70

^a When a Mn²⁺:Mn⁴⁺ ratio of 1:1 is assumed.

as the reference compound Mn(CH₃COO)₂·4H₂O, it is assumed that they still consist of isolated species that experience minor spin–spin coupling (decreased fine and hyperfine structures) but that give rise to the same ESR intensity as isolated Mn atoms in the reference compound.

An indication of the total amount of isolated manganese species is obtained from the ESR signals after reduction, when all manganese species are reduced to ESR-active Mn²⁺. In addition, a quantitative distribution of oxidation states of calcined samples is obtained using two conclusions drawn from TPR patterns:¹⁶

(1) After calcination, the *average* oxidation state of the catalysts is 3+; hence, Mn²⁺ and Mn⁴⁺ are present in a 1/1 ratio.

(2) After reduction at 930 K, all manganese species are present as Mn²⁺.

Table 1 shows the molar amount of paramagnetic manganese species present before and after reduction at 930 K according to the above-stated assumptions. For the calcined 0.5 wt % loaded catalyst, about two-thirds of the amount of manganese present was observed by ESR, whereas almost all the manganese is detected after reduction. Hence, it is reasonable to state that almost all the manganese species are isolated and that one-third was present as isolated Mn³⁺ after calcination. For the 2 wt % loading, a much lower fraction of paramagnetic species is observed after calcination, whereas more than 80% is detected by ESR after reduction. This means that the amount of isolated manganese species is slightly lower compared with the 0.5 wt % sample, while the relative content of Mn³⁺ is considerably larger. At 4.5 wt % loading, the amount of paramagnetic species after calcination is low, while the reduced samples give rise to strong ESR signals, which shows that most of the manganese is present as Mn³⁺ and that this fraction is mainly isolated.

3.3. Catalytic Tests. In the Introduction, the aim to find a relation between the structure of the catalysts and the selectivity toward N₂ production for the SCR reaction was underlined. The selectivity is mainly determined by the ratio at which the following possible reactions proceed:

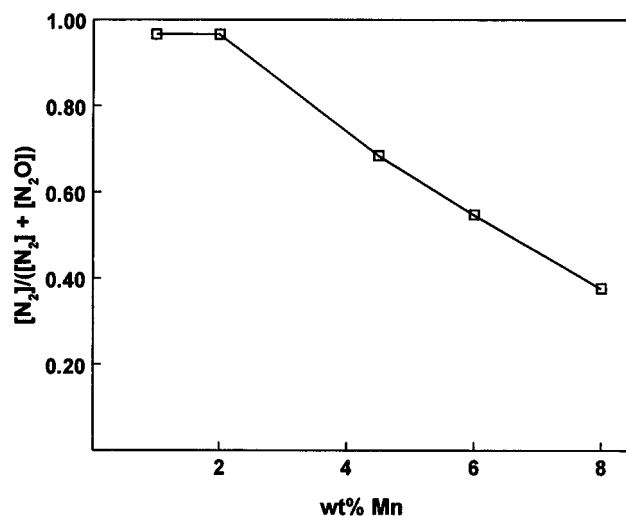
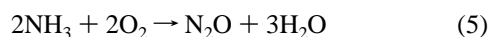
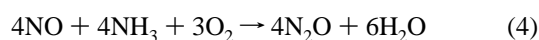
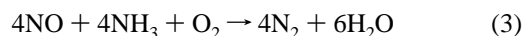


Figure 9. Selectivity toward N₂ production in the selective catalytic reduction of NO at 523 K as a function of Mn loading.

As reaction 3 is desired, the selectivity is defined as the following ratio of product concentrations:

$$S = \frac{[\text{N}_2]}{[\text{N}_2] + [\text{N}_2\text{O}]} \quad (6)$$

Figure 9 shows the selectivities during catalytic tests at 523 K of the 1–8 wt % Mn/Al₂O₃ catalysts. Up to 2 wt % Mn loading, the selectivities are higher than 96%. Above this loading, the selectivities drop strongly and almost linearly with loading, leading to a very poor selectivity at 8 wt % Mn loading.

4. Discussion

4.1. Interaction of Manganese Ions with Support. UV-vis spectroscopy shows that [Mn(H₂O)₆]²⁺ is the precursor molecule present in the impregnation solution. Hence, a metal–support interaction has to arise from a reaction of this complex with surface hydroxyls of the γ -Al₂O₃ support. The solution has a pH in the range 6.7–7.5, depending on the concentration of the precursor salt. Kapteijn *et al.*¹⁶ stated that upon impregnation, acidic hydroxyls (slightly positively charged) have an electronic interaction with the oxygen atom of the water molecules of the hexaaquo complex. As soon as these hydroxyls are consumed, the (slightly negative) basic hydroxyls react with the positively charged Mn ions. According to the present spectra of the overtones of the surface hydroxyls (Figure 2), there is no preference of the hexaaquo complex to react with acidic or basic hydroxyls. Hence, both interactions described by Kapteijn *et al.* can be confirmed, but they proceed simultaneously rather than in sequence.

After drying at 393 K, the γ -Al₂O₃ support contains about 10–11 OH groups nm⁻².²⁴ If every Mn ion would react with 1 OH of the support, the hydroxyls would be consumed at 16.8 wt % Mn loading. If the reaction would proceed at a 1/2 ratio, complete depletion of hydroxyls would be reached at 8.4 wt % loading. Figure 3 clearly shows that the amount of hydroxyls has decreased by about 50% at 4.5 wt % Mn loading. Hence, the assumption that the reaction of Mn ions with surface hydroxyls takes place at a 1/2 ratio is proven quantitatively now by DRS results, and multilayer formation can be excluded up to that loading. Up to 4.5 wt % Mn loading, surface hydroxyls are titrated by the Mn complex, giving rise to a linear decrease

TABLE 2: ESR Parameters of Mn-Containing Reference Compounds

Mn ⁿ⁺	loading	environment	symmetry	<i>g</i>	10 ⁻⁴ <i>A</i> /cm ⁻¹	10 ⁻⁴ <i>D</i> /cm ⁻¹	ref
Mn ²⁺	1–6 wt %	γ-Al ₂ O ₃	tetrahedral/octahedral	2.00	76.6	br distribution	14
Mn ²⁺		γ-Al ₂ O ₃	octahedral		86.8	270–1350	26
Mn ²⁺	4.3 wt %	Al ₂ O ₃	cubic	2.0023	86.9		15
Mn ²⁺	0.1–1.7 wt %	Na-A; Li-A	octahedral	2.006	89.0	100	27
Mn ²⁺	3 mol%	MnOH ZSM	tetrahedral	4.27			34
Mn ²⁺	1 ppm	MgO polycrystalline	axial	2.0064	81.2	52–85	28, 32
Mn ⁴⁺	0.001–0.1 atom %	α-Al ₂ O ₃	axial	1.9937	71.1		18
Mn ⁴⁺		MgO polycrystalline		1.9970	70.7	–1957	32
Mn ⁴⁺	0.1%	MgO–LiO	axial	1.995	70.0	280	33

of the bands of the OH overtones (Figure 3) with Mn loading. Above 4.5 wt % loading, deposition of the Mn hexaquo complex as well as reaction with the surface hydroxyls takes place, causing a less than linear decrease of the bands of the OH overtones.

It should be noted that the use of the acetate precursor may be important for the obtained dispersion of the manganese. Alumina-supported manganese oxides, prepared *via* impregnation from the nitrate solution, yield XRD lines at lower loadings (>2 wt %)^{10,14} than *via* impregnation from the acetate precursor (>8.4 wt %).^{11,16} An important difference between these impregnation solutions is the acidic pH of the nitrate solution *vs* the neutral pH (6.7–7.5) of the acetate solution. Possibly, this neutral pH provides the condition at which most of the hydroxyls participate in the anchoring process. Baltanás *et al.*¹ prepared catalysts *via* the nitrate precursor and added a NH₄-OH solution directly after impregnation, inducing simultaneously an increase in pH and precipitation of MnOH, resulting in a better dispersed oxidic manganese layer, not detectable by XRD up to 4.8 wt % loading.

4.2. Oxidation State and Coordination Manganese Species. The average oxidation state of the calcined catalysts is about Mn³⁺, irrespective of the Mn loading.¹⁶ The ESR spectra show that not all manganese is present as a 3+ species because Mn³⁺ exhibits no ESR signal.¹⁷ Hence, next to Mn³⁺, both Mn²⁺ and Mn⁴⁺ species must be present to account for the average oxidation state, and the observed ESR spectrum must be due to one or both of these species. In Table 2, some ESR parameters are presented of reference compounds. Mn²⁺ species, in various coordinations, have been much more extensively studied than Mn⁴⁺ species. Two general spectral differences between the two oxidation states are evident. Firstly, the reported *g* values for Mn⁴⁺ are slightly less than 2, whereas those of Mn²⁺ are slightly above 2. Secondly, the value of *A* ranges from 65 × 10⁻⁴ to 71 × 10⁻⁴ cm⁻¹ for Mn⁴⁺ and from 75.7 × 10⁻⁴ to 91.6 × 10⁻⁴ cm⁻¹ for Mn²⁺. By consequence, both the *A* and *g* values observed in the recorded ESR spectra can likely be assigned to Mn²⁺. However, spectral simulation indicated that the recorded spectra do not result from one paramagnetic species. As the average oxidation state of the samples is 3+,^{7,16} the observed Mn²⁺ signal is possibly superimposed on a Mn⁴⁺ signal.

The appearance of broad wings around the central absorption in the ESR spectra of Mn²⁺ containing materials was observed previously by other authors.^{15,26–28} The wings are due to dipole–dipole interactions,¹⁵ and as a result, they are predominant in the spectra of higher loaded samples. Besides, they become the predominant feature in the spectra of low-loaded samples during reduction as the amount of Mn²⁺ increases (Figure 8), in line with the spectral changes reported on reduced MnO_x/Al₂O₃ by Baltanás *et al.*¹⁵

Table 3 presents some literature data on the absorption bands of d–d transitions of Mn ions in different environments. From this table, it is clear that Mn³⁺ and Mn⁴⁺ show mainly one d–d

TABLE 3: Absorption Maxima of d–d Transitions of Mn-Containing Reference Compounds

Mn ⁿ⁺	environment	absn max/cm ⁻¹	transition	ref
Mn ²⁺	MnO	16 400	⁴ T ₂ ← ⁶ A ₁	30
		20 800	⁴ T ₂ ← ⁶ A ₁	
		23 800	⁴ A ₁ ← ⁶ A ₁	
Mn ²⁺	Mn(Ac) ₂ ·4H ₂ O	18 500	⁴ T ₂ ← ⁶ A ₁	35
		22 700	⁴ T ₂ ← ⁶ A ₁	
		24 740	⁴ A ₁ ← ⁶ A ₁	
		18 700	⁵ T _{2g} ← ⁵ E _g (L)	
Mn ³⁺	Al ₂ O ₃	20 600	⁵ T _{2g} ← ⁵ E _g (II)	19
		21 000	⁵ T _{2g} ← ⁵ E _g	
Mn ³⁺	CsMn(SO ₄)·2.12H ₂ O	21 000	⁵ T _{2g} ← ⁵ E _g	29
Mn ³⁺	Mn–APO-34	20 400	⁵ T _{2g} ← ⁵ E _g	36
Mn ⁴⁺	Al ₂ O ₃	21 300	⁴ T _{2g} ← ⁴ A _{2g}	18

transition, while Mn²⁺ shows up to six transitions (although only three of them are visible in solids)^{25,29} which are all spin forbidden and by consequence very weak. As the literature data show almost all band maxima to be located in the 20 000–25 000-cm⁻¹ range, assignment of the bands observed in Figure 1 is rather cumbersome.

TPR data show that reduction of MnO_x/Al₂O₃ catalysts, prepared *via* the acetate precursor, proceeds in a broad temperature range (480–900 K).¹⁶ Hence, it may be assumed that after reduction at 930 K for 2 h, all species are completely reduced to Mn²⁺ and the very weak band at 23 700 cm⁻¹ (Figure 4d) can thus be assigned to the ⁴A₁ ← ⁶A₁ transition in Mn²⁺.³⁰ Therefore, the band observed at 20 000–22 500 cm⁻¹ in all the other spectra can be assigned only to the ⁵T_{2g} ← ⁵E_g transition in Mn³⁺/Al₂O₃^{19,31} and/or the ⁴T₂ ← ⁴A₂ transition in Mn⁴⁺/Al₂O₃.¹⁸ The DRS spectrum of the dried, uncalcined catalyst (Figure 1a) shows this band, indicating that oxidation of the Mn²⁺ ion of the precursor already proceeds during drying, and not only during calcination. However, the band becomes more intense during calcination, as more Mn²⁺ ions are oxidized to higher oxidation states. During calcination, the band is centered at 21 000–21 300 cm⁻¹, in-between the reported values of Mn³⁺ and Mn⁴⁺ on an Al₂O₃ support.

The gradually decreasing intensity of the spectrum during reduction corresponds fairly well to the TPR results,¹⁶ which show broad reduction peaks, covering almost the entire temperature range.

Most of the ESR studies on Mn²⁺-containing materials report an octahedral or an axially distorted octahedral coordination of Mn²⁺ ions.^{14,18,24–26,32–34} Wichterlová *et al.*³⁴ report an ESR signal of Mn²⁺ in a distorted tetrahedron at *g* = 4.27. Literature data presented in Table 2 suggest the coordination of the Mn²⁺ ions observed in the recorded ESR spectra to be most reasonably described as axially distorted octahedral.

4.3. Fraction of Isolated Manganese Species: Quantitative Distribution of Oxidation States. The Curie–Weiss plots in Figure 6 show that up to 4.5 wt % Mn loading, at least part of the manganese species is present in the form of isolated species. The high molar fraction of paramagnetic manganese

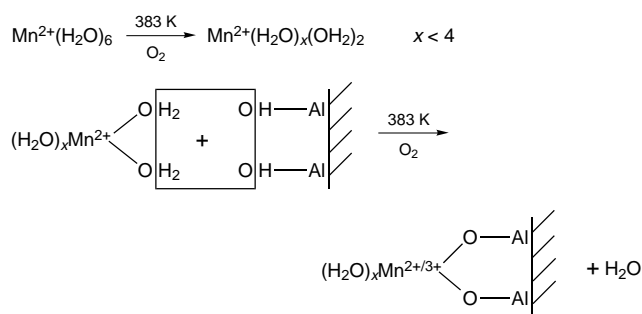
after reduction (Table 1) indicates that up to 4.5 wt % loading, the fraction of isolated manganese is indeed very high, approaching 100% at 0.5 wt % Mn loading. Moreover, from the fact that the intercept with the x axis is comparable for the low-loaded samples, it is concluded that the paramagnetically active manganese species behave comparably for these samples. At higher loadings, no linear fit can be obtained, meaning that all paramagnetic manganese species are influenced by neighboring sites. The loading above which isolated species are no longer present coincides with the loading above which manganese ions no longer interact exclusively with surface hydroxyls of the support (Figure 3). Note that even at loadings beyond 5 wt %, the manganese dispersion remains high, as no microcrystallites are observed by XRD and as XPS data point toward a strong metal–support interaction.¹⁶ It is assumed that two-dimensional layers of manganese oxides are formed at these higher loadings.¹⁶

For *calcined samples*, the amount of paramagnetic manganese as a function of loading (Figure 7) shows that the fraction of manganese species present as isolated paramagnetic species decreases sharply for loadings increasing from 0.5 to 4.5 wt %. In contrast, for *reduced samples* the amount of paramagnetic manganese slightly decreases as a function of loading. This shows that, for calcined samples, the fraction of ESR-silent Mn³⁺ sharply increases with Mn loading. The results correspond fairly well to those from ESR studies by Lo Jacono *et al.*,¹⁴ who showed that at low loadings (0.5 wt %) about 35% of the manganese was present as Mn²⁺. At higher loadings, the absolute signal of Mn²⁺ did not increase, whereas the relative content of Mn³⁺ increased significantly. Hence, it appears that only a limited amount of manganese can be stabilized as Mn²⁺ on the Al₂O₃ surface. Additional manganese is oxidized to Mn³⁺ and to a lesser extent to Mn⁴⁺.

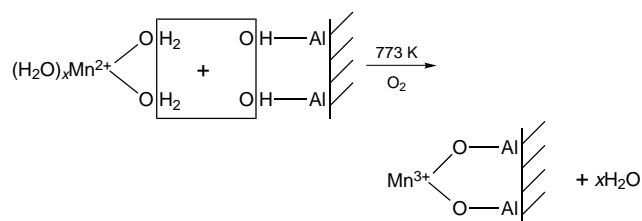
In summary, it can be concluded that at manganese loadings of less than 1 wt %, practically all manganese species are isolated on the Al₂O₃ support and that after calcination, the ratio Mn²⁺:Mn³⁺:Mn⁴⁺ is approximately 1:1:1. At increased loading, two-dimensional layers of manganese are formed in addition to isolated species and the fraction Mn³⁺ becomes much larger. At 6 wt % and higher loadings, no Mn species are isolated and dispersed two-dimensional layers cover the Al₂O₃ surface.

The selectivity of the catalysts in the selective catalytic reduction of NO decreases significantly with the Mn loading. Apparently, catalysts containing mainly isolated Mn species (0.5 wt %) on the surface are exclusively active for the desired reaction (3). At 2 wt % Mn loading, not all Mn species are isolated but the selectivity is still close to unity, showing that active sites for the desired reaction do not have to be perfectly (magnetically) isolated species. This idea is supported by the fact that at 7 wt % loading, hardly any isolated Mn species are present (Figure 6), whereas the desired reaction still proceeds at a certain rate. However, the general trend is that increasing amounts of two-dimensional manganese oxide layers, present at higher loadings, cause an increasing contribution of the undesired reactions (4) and (5). Hence, the selective reaction (3) proceeds over (magnetically) isolated Mn species and very small clusters, whereas reactions 4 and 5 require larger Mn ensembles. From a selectivity point of view, the Mn loading of this type of catalysts should not exceed 2 wt %.

4.4. Reaction Scheme for the Preparation Al₂O₃-Supported Manganese Oxides. The Mn(H₂O)₆ complex is the precursor molecule present in an aqueous solution of manganese acetate. During impregnation and subsequent drying, the reaction of this complex with both the acidic and basic hydroxyls of the γ -Al₂O₃ support can be represented as follows:



Upon calcination, further oxidation of the manganese occurs:



It should be noted that Mn³⁺ is the average oxidation state after calcination and that its relative content increases with increasing Mn loading.

5. Conclusions

From this study by ESR and DRS of alumina-supported manganese oxides, prepared from the acetate precursor, the following conclusions can be drawn:

During impregnation of the aqueous precursor solution, the [Mn(H₂O)₆]²⁺ complex reacts with the surface hydroxyls of the Al₂O₃ support. Evidence was obtained for a stoichiometry of Mn/OH = 1/2 for this reaction. At loadings above approximately 5 wt %, the reaction with surface hydroxyls is accompanied by deposition of the precursor complex.

The preparation method yields a highly dispersed catalyst with a high percentage (above 70%) of isolated species up to 4.5 wt % manganese loading. Part of the manganese is oxidized to higher oxidation states upon drying at 383 K, while a significant increase in the average oxidation state takes place during further calcination at 573 K. The manganese oxides obtained are present as a mixture of Mn²⁺, Mn³⁺, and Mn⁴⁺. At low loadings, these oxidation states are present in a ratio of around 1:1:1, while at higher loadings Mn³⁺ is the dominant species. The fraction Mn²⁺ is present in an axially distorted octahedral coordination.

The observed decrease in selectivity for the selective catalytic reduction of NO as a function of Mn loading in these materials corresponds to the general trend of decreasing content of magnetically isolated Mn species with loading. However, sites exclusively active for the desired reaction toward N₂ production do not have to be perfectly isolated. At increasing content of dispersed two-dimensional manganese oxide layers, the contribution of undesired reactions strongly increases. Hence, larger Mn ensembles are apparently necessary for the unselective reaction pathway.

Acknowledgment. Financial support from the Dutch Foundation for Chemical Research (SON) is gratefully acknowledged. B.M.W. thanks the Belgian National Fund for Scientific Research (NFWO) for a grant as research assistant. Prof. F. E. Mabbs (University of Manchester, U.K.) is acknowledged for performing Q-band and K-band ESR measurements and D. S. Brands for performing the selectivity experiments.

References and Notes

- (1) Baltanás, M. A.; Stiles, A. B.; Katzer, J. R. *Appl. Catal.* **1986**, *28*, 13.
- (2) Il'chenko, N. I.; Godolets, G. I. *J. Catal.* **1975**, *39*, 57.
- (3) Karlsson, H. T.; Rosenberg, H. S. *Ind. Eng. Chem. Process Res. Dev.* **1984**, *23*, 808.
- (4) Van der Kleut, D. Ph.D. Thesis, University of Utrecht, The Netherlands, 1994.
- (5) Nishino, A. *Catal. Today* **1991**, *10*, 107.
- (6) Lo Jacono, M.; Schiavello, M. *Preparation of Catalysts*; Delmon, B., Jacobs, P. A., Poncelet, G., Eds.; Elsevier: Amsterdam, 1976; p 474.
- (7) Singoredjo, L.; Korver, R.; Kapteijn, F.; Moulijn, J. A. *Appl. Catal. B: Environ.* **1992**, *1*, 297.
- (8) Singoredjo, L. Ph.D. Thesis, University of Amsterdam, The Netherlands, 1992.
- (9) Kijlstra, W. S.; Daamen, J. C. M. L.; Van de Graaf, J. M.; Van der Linden, B.; Poels, E. K.; Bliet, A. *Appl. Catal. B: Environ.* **1996**, *7*, 237.
- (10) Strohmeier, B. R.; Hercules, D. M. *J. Phys. Chem.* **1984**, *88*, 4922.
- (11) Wang, W.; Yang, Y.; Zhang, J. *Appl. Catal. A* **1995**, *131*, 189.
- (12) Baltanás, M. A.; Stiles, A. B.; Katzer, J. R. *J. Catal.* **1984**, *88*, 362.
- (13) Selwood, P. W.; Moore, T. E.; Ellis, M.; Wethington, K. *J. Am. Chem. Soc.* **1949**, *71*, 693.
- (14) Lo Jacono, M.; Schiavello, M.; Cordischi, D.; Mercanti, G. *Gazz. Chim. Ital.* **1975**, *105*, 1165.
- (15) Baltanás, M.; DeCanio, S. J.; Katzer, J. R.; Dybowski, C. *Acta Chim. Hung.* **1985**, *116*, 285.
- (16) Kapteijn, F.; Van Langeveld, A. D.; Moulijn, J. A.; Andreini, A.; Vuurman, M. A.; Turek, A. M.; Jehng, J.-M.; Wachs, I. E. *J. Catal.* **1994**, *150*, 94.
- (17) Mn^{3+} is not detected in ESR due to complete splitting of energy levels (no ground-state degeneracy). If these splittings are very large (1 cm^{-1}) no ESR signal is observed. Védrine, J. C. *Characterisation of Heterogeneous Catalysts*; Delannay, F., Ed.; Dekker: New York, 1984; p 161.
- (18) Geschwind, S.; Kisliuk, M. P.; Remeika, J. P.; Wood, D. L. *Phys. Rev.* **1962**, *126*, 1684.
- (19) McClure, D. S. *J. Chem. Phys.* **1962**, *36*, 2757.
- (20) Heidt, L. J.; Koster, G. F.; Johnson, A. *J. Am. Chem. Soc.* **1959**, *80*, 6471.
- (21) QPOW: ESR simulation package written by M. Nilges, and the Illinois EPR Research Center, University of Illinois at Urbana-Champaign.
- (22) Schoonheydt, R. A.; Velghe, F.; Baerts, R.; Uytterhoeven, J. B. *Clays Clay Min.* **1979**, *27*, 2.
- (23) Schoonheydt, R. A. *Characterisation of Heterogeneous Catalysts*; Delannay, F., Ed.; Dekker: New York, 1984; p 125.
- (24) Knözinger, H.; Ratnasamy, P. *Catal. Rev.-Sci. Eng.* **1978**, *17*, 31.
- (25) Bleaney, B.; Ingram, D. J. E. *Proc. R. Soc. London* **1951**, *A205*, 336.
- (26) Burlamacchi, L.; Villa, P. L. *React. Kin. Catal. Lett.* **1975**, *3*, 199.
- (27) De Vos, D. E.; Weckhuysen, B. M.; Bein, T. *J. Am. Chem. Soc.* **1996**, *118*, 9615.
- (28) Derouane, E. G.; Thielen, J.; Indovina, V. *Bull. Soc. Chim. Belg.* **1973**, *82*, 657.
- (29) Holmes, O. G.; McClure, D. S. *J. Chem. Phys.* **1957**, *26*, 1686.
- (30) Pratt, G. W.; Coelho, R. *Phys. Rev.* **1959**, *116*, 281.
- (31) Fackler, J. P.; Chawla, I. D. *Inorg. Chem.* **1964**, *3*, 1130.
- (32) Derouane, E. G.; Indovina, V. *Bull. Soc. Chim. Belg.* **1973**, *82*, 645.
- (33) Henderson, B.; Hall, T. P. P. *Proc. Phys. Soc.* **1967**, *90*, 511.
- (34) Wichterlová, B.; Beran, S.; Bednarová, S.; Nedomová, K.; Dudíková, L.; Jíru, P. *Innovation in Zeolite Materials Science*; Grobet, P. J., Ed.; Elsevier: Amsterdam, 1988; p 199.
- (35) Mehra, A.; Venkateswarlu, P. *J. Chem. Phys.* **1968**, *48*, 4381.
- (36) Rajic, N.; Stojakovic, D.; Hocevar, S.; Kaucic, V. *Zeolites* **1993**, *13*, 3849.